AIAA 81-1925R

Theoretical Analysis of Parachute Inflation Including Fluid Kinetics

James W. Purvis*
Sandia National Laboratories, Albuquerque, N. Mex.

An analysis is presented for predicting parachute inflation. Equations of motion for the complete system are developed from first principles, and are solved with no experimental inputs. Ballistic equations of motion are derived for the canopy, payload, and suspension line masses. However, the enclosed fluid mass is not lumped with the canopy as an apparent mass term. Instead, the fluid conservation equations for a deforming, accelerating control volume are solved to determine the behavior of the captured fluid and its interaction with the canopy. Only first-order effects are included, and the analysis is limited to inviscid, incompressible flow. Results for both porous and nonporous canopies are compared with experimental data.

Nomenclature

A_{SL} = cross-sectional area of suspension line
E_{SL} = elastic modulus of suspension line
G = inverse square of axial Froude number $= sg\cos\phi / V_\infty^2$
g = gravitational constant
m = mass
N_{SL} = number of suspension lines
P = momentum
p = pressure, or nondimensional momentum in Eqs. (25-28)
Q = nondimensional pressure function, Eq. (30)
q_{rel} = relative dynamic pressure
R = nondimensional radius or length $= r/s$
r = radial coordinate
S_{LL} = suspension line length
s = constructed length of canopy radial (used as reference length)
T = tension
t = time
u = velocity
v = nondimensional velocity
x = axial coordinate
α = angle of attack
η_L = suspension line mass ratio $= m_L/m_c$
η_B = forebody mass ratio $= m_B/m_c$
θ = angular coordinate
λ = geometric porosity
$\bar{\lambda}$ = porosity parameter $= 1-\lambda$
μ = air mass ratio $= \pi\rho s^3/2m_c$
ξ = axial integration variable
ρ = fluid density
σ = nondimensional tension $= 2T/\rho_\infty V_\infty^2 \pi s^2$
τ = nondimensional time $= V_\infty t/s$
ϕ = angle of gravity vector
Ψ = suspension line angle

Subscripts

B = body
c = canopy
i = inlet
m = average at canopy
R,r = radial
s = skirt
v = vent
x = axial
$1,2$ = locations defined in figures
∞ = freestream

Received March 9, 1981; revision received July 20, 1981; presented as Paper 81-1925 at the AIAA 7th Aerodynamic Decelerator and Balloon Technology Conference, San Diego, Calif., Oct. 21-23, 1981.

*Member of Technical Staff, Aerodynamic Department 5630. Member AIAA.

Introduction

THE performance of a parachute-payload system may be analytically determined by integrating the flight-path equations of motion. To do so accurately requires that the shape of the parachute and its associated loads as a function of time, i.e., the inflation history, be known or computed simultaneously. The inflation problem involves an unsteady, viscous flow with boundary conditions applied on a porous elastic surface whose instantaneous definition is determined by the flowfield. Because of the nature of the surface and the complex interaction with the flow, simplifications such as those applied in classical aircraft aeroelastic problems cannot be made.

In spite of these problems, a considerable number of analytical methods have been developed. These methods may be loosely grouped in three categories: lumped mass kinetic methods, fluid kinetic inflation studies, and combinations of the two. The more significant theories are mentioned in the survey by Pepper and Maydew,[1] the inflation theory discussion by Roberts and Reddy,[2] and the comprehensive Air Force Recovery Systems Design Guide.[3]

In the lumped mass approach, flight-path kinetic equations are developed for the payload mass and one or more mass points representing the parachute. The important influences of canopy shape and inflation forces, which are the principal unknowns driving the system, are largely determined from empirical methods rather than calculated as part of the problem. The inflation rate is generally obtained by solving a conservation of mass equation for the canopy internal volume. Use of the continuity equation for inflation rate includes both filling time and filling distance theories, such as those of Muller,[4] Scheubel,[5] O'Hara,[6] and Heinrich.[7]

As Wolf[8] has stated, the use of continuity inherently restricts inflation theories, since empirical inputs are required insofar as conservation of mass is a kinematic statement of fluid effects. In reality, fluid kinetics determine the canopy inflation, the driving force being the radial component of conservation of momentum. These concepts were introduced by Weinig,[9] and later used by Toni.[10] The effects of fluid motion and unsteady pressure loadings were lumped into "radial force coefficients" and "apparent mass effects,"

which were determined empirically rather than being solved for analytically. The most effective applications of these ideas appear to be the procedures developed by McVey and Wolf,[11] and Fu.[12]

Once the importance of the interaction between the flowfield and canopy kinetics was recognized, several fluid kinetic inflation studies followed. Roberts[13] examined the inflation of a massless parabolic shell, and calculated the unsteady pressure distribution in the presence of starting vortices. Klimas[14] used a classical vortex sheet approach to examine internal parachute flows, and later to predict inflating canopy differential pressures.[15] Reddy and Roberts[16] analyzed the inflation of a massless, multiple-plate canopy representation in two-dimensional incompressible flow. None of the above investigators, however, coupled their fluid kinetic methods with canopy and payload kinetics.

The objective of the present paper is to develop a simple analytical model for predicting canopy inflation, using a minimum number of degrees of freedom. The equations of motion for the parachute-payload system and the captured fluid behavior during the inflation process are derived from first principles, with no experimental inputs. Only first-order effects are included, and the analysis is limited to inviscid, incompressible flow. To the author's knowledge, this is the first time that the dynamics equations for the parachute system and the conservation equations for the enclosed fluid have been solved simultaneously. Results of the analysis for porous and nonporous canopies are compared to experimental data, and model deficiencies are discussed. Proposals for extensions of the basic approach to more detailed models are also presented.

Analysis

The first step in the analysis involves a decision on whether the detailed canopy shape will be solved for, as in the finite-element models, or whether a specific geometric form will be assumed, and the time varying dimensions of the form solved for. In keeping with the objectives of simplicity and minimum degrees of freedom, and in light of the excessive computation times of finite-element models, the latter approach was chosen.

Several assumed forms have been used in past work. Scheubel[5] investigated a family of cylinders, while O'Hara[6] assumed the canopy to be a truncated cone. Heinrich[7] considered a modified O'Hara model, consisting of a truncated cone terminated by a hemisphere; Payne[17] assumed a cylinder shape for his internal flow studies; and Wilcox[18] used a cylinder terminated by a hemisphere.

Of the available forms, the cylinder shape is the most appealing. The sides of the cylinder are aligned with radial coordinate axes, which is most convenient from a fluid dynamic computational standpoint; and a single parameter, the instantaneous radius, defines the shape. Additionally, as shown in Fig. 1, a cylinder closely approximates the overall parachute shape during the entire inflation process.

The cylindrical coordinate system and the pertinent simulation parameters used in this analysis are shown in Fig. 2. In the discussion which follows, the rear (vertical) portion of the parachute will be referred to as the canopy, and the horizontal (tube) portion will be referred to as the skirt.

The equations of motion for the system may be separated into two groups—rigid body, or point mass dynamics, and fluid mechanics. The rigid body equations are written for the forebody, suspension lines, skirt, and canopy in the usual manner. The fluid mechanics equations consist of conservation of mass, axial momentum, and radial momentum for the air mass enclosed by the cylindrical surface representing the parachute. The rigid body equations will be developed first.

The development of the equation for the time rate of change of the radial momentum of the skirt will be used to illustrate the procedure and the nondimensionalization

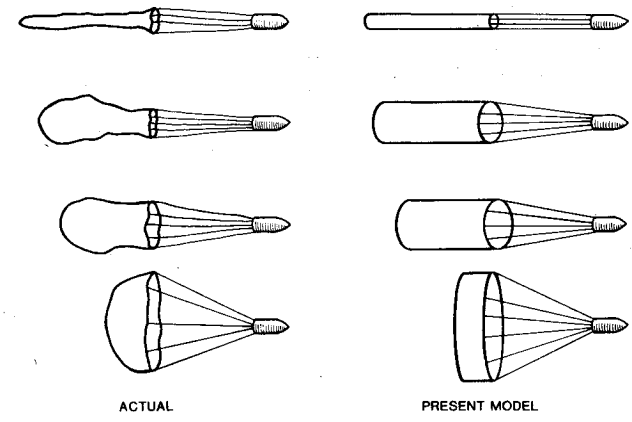

Fig. 1 Parachute shapes during inflation.

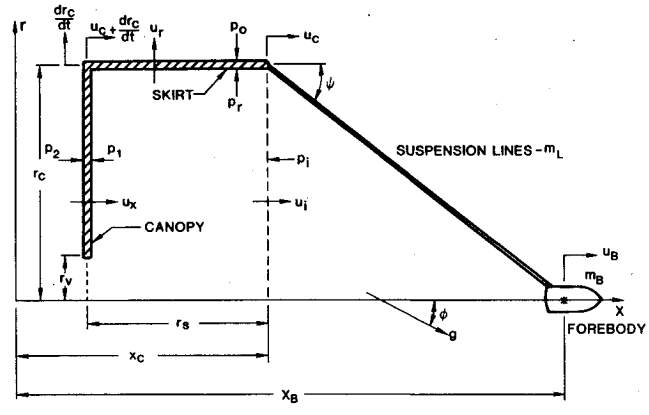

Fig. 2 Simulation parameters and coordinate system.

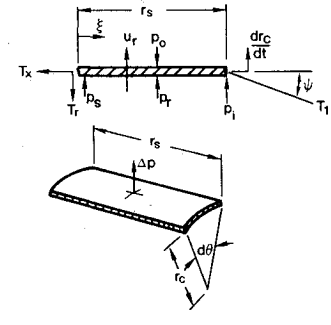

Fig. 3 Freebody diagram of skirt element.

process. A freebody diagram of a differential strip of the skirt is shown in Fig. 3. The assumptions concerning the skirt and its motion are 1) constant mass density per unit length, 2) inextensible canopy material, 3) linear axial variation in differential pressure, 4) the skirt does not rotate, and 5) hoop stresses are negligible. Using assumptions 1 and 4, the momentum of the element is

$$P_r = \frac{\mathrm{d}r_c}{\mathrm{d}t}\,\mathrm{d}m = \left(\frac{m_c}{s}\right)\left(\frac{\mathrm{d}\theta}{2\pi}\right)\frac{\mathrm{d}r_c}{\mathrm{d}t}\,r_s \tag{1}$$

and the radial force is

$$F_r = \bar{\lambda} r_c \mathrm{d}\theta \int_0^{r_s} \Delta p\,\mathrm{d}\xi - (T_r + T_1 \sin\Psi)\,(\mathrm{d}\theta/2\pi) \tag{2}$$

With the linear differential pressure assumption,

$$\Delta p(\xi) = \Delta p_s + (\Delta p_i - \Delta p_s)\,(\xi/r_s) \tag{3}$$

The radial tension at the skirt-canopy junction is solved for by enforcing the zero moment assumption at the centroid of the element:

$$0=T_r\left(\frac{r_s}{2}\right)\left(\frac{\mathrm{d}\theta}{2\pi}\right)-T_l\sin\Psi\left(\frac{r_s}{2}\right)\left(\frac{\mathrm{d}\theta}{2\pi}\right)+\bar{\lambda}\int_0^{r_s}\Delta p(r_s\mathrm{d}\theta)\left(\xi-\frac{r_s}{2}\right)\mathrm{d}\xi \tag{4}$$

which gives

$$T_r=T_l\sin\Psi-\frac{\pi r_c r_s}{3}\bar{\lambda}(\Delta p_i-\Delta p_s) \tag{5}$$

Equating $\mathrm{d}P_r/\mathrm{d}t$ to F_r, performing the differentiations, and using the above equations gives

$$\left(\frac{m_c}{s}\right)\left[\frac{\mathrm{d}^2r_c}{\mathrm{d}t^2}r_s-\left(\frac{\mathrm{d}r_c}{\mathrm{d}t}\right)^2\right]=\frac{2}{3}\bar{\lambda}\pi r_c r_s(2\Delta p_i+\Delta p_s)-2T_l\sin\psi \tag{6}$$

where the relation between r_s, r_c, and the constructed radial length s (= const) was used:

$$r_c+r_s=s \tag{7}$$

Nondimensionalizing gives

$$(1-R_c)\ddot{R}_c=\dot{R}_c^2+\tfrac{2}{3}\bar{\lambda}\mu R_c(1-R_c)(2\Delta Q_i+\Delta Q_s)-2\mu\sigma_l\sin\psi \tag{8}$$

where the dot signifies differentiation with respect to the nondimensional time parameter τ, and all lengths are nondimensionalized by the canopy radial length s. The pressure loading functions ΔQ_i and ΔQ_s differ for porous and nonporous chutes, and will be developed later.

The radial momentum equation for the suspension lines can be developed similarly using the assumption of a linear radial velocity distribution along the lines. In nondimensional form, the equation is

$$\tfrac{1}{2}\eta_L\ddot{R}_c=\mu(\sigma_l-\sigma_2)\sin\psi \tag{9}$$

where σ_2 is the nondimensional tension in the suspension lines at the point where the lines connect to the forebody. Combining Eqs. (8) and (9) to eliminate σ_l gives the desired equation of motion for the canopy radius:

$$\ddot{R}_c=[\dot{R}_c^2+\tfrac{2}{3}\bar{\lambda}\mu R_c(1-R_c)(2\Delta Q_i+\Delta Q_s)-2\mu\sigma_2\sin\Psi]\times[1-R_c+\eta_L]^{-1} \tag{10}$$

Note that the suspension line mass ratio ensures that the equation is nonsingular. The tension in the lines is found from

$$T_2=E_{\mathrm{SL}}A_{\mathrm{SL}}N_{\mathrm{SL}}\left(\frac{S_{\mathrm{LL}}-S_{\mathrm{LL}_0}}{S_{\mathrm{LL}_0}}\right) \tag{11}$$

where S_{LL_0} is the unloaded length of a line and

$$S_{\mathrm{LL}}=\sqrt{(x_B-x_c)^2+r_c^2} \tag{12}$$

Also,

$$\sin\Psi=r_c/S_{\mathrm{LL}},\quad \cos\Psi=(x_B-x_c)/S_{\mathrm{LL}} \tag{13}$$

Axial momentum expressions for the canopy, skirt, suspension lines, and forebody can be combined to yield acceleration equations for the forebody and the canopy. The suspension lines are again assumed to have a linear velocity distribution, and forebody drag is neglected. (Forebody drag area is generally an order of magnitude smaller than parachute drag area.) Momentum time derivative expressions for the canopy and skirt are combined to eliminate the unknown tension T_x at the skirt-canopy juncture. Similarly, suspension line and forebody equations are combined to eliminate one of the tension terms. The resulting equations in nondimensional form are

$$\dot{v}_C=-(\dot{R}_c^2+R_c\ddot{R}_c)+\mu\sigma_l\cos\Psi+G-\mu\bar{\lambda}R_c^2\Delta Q_c \tag{14}$$

and

$$\dot{v}_B=\frac{-\tfrac{1}{2}\eta_L\dot{v}_c+(\eta_L+\eta_B)G-\mu\sigma_l\cos\Psi}{\eta_B+\tfrac{1}{2}\eta_L} \tag{15}$$

The differential pressure loading function ΔQ_c again depends on whether or not the parachute is porous, and will be developed later. The nondimensional tension σ_l is assumed to be equal to σ_2, which is approximately the case for suspension line materials such as Kevlar and nylon.

Equations (10), (14), and (15), with the auxiliary relations (11-13), are the necessary dynamics equations for R_c, v_c, and v_B. To integrate these equations requires that the pressure loading functions ΔQ_i, ΔQ_s, and ΔQ_c be known. In most formulations, such as those of Heinrich[7] and McVey and Wolf,[11] expressions similar to Eqs. (10), (14), and (15) are derived in a similar straightforward manner, but the pressure loadings, in the form of drag and radial force coefficients, are input from experimental data. In the present approach, equations will be developed, from fluid dynamics expressions, which can be solved to yield the required air mass velocities, and hence pressure functions.

Fluid dynamics equations must be solved for three unknowns: u_i, u_x, and u_r. These are the enclosed air mass velocities which, in effect, determine the pressure loadings on the canopy and skirt. Solving these equations simultaneously with the rigid body dynamics equations will correctly account for the exchange of momentum (through the pressure terms) between parachute and fluid that has been labeled apparent mass effects, as well as providing the pressure loadings necessary for computing drag and radial forces.

The fluid equations are derived for the fluid contained in the time-varying control volume shown in Fig. 4, which is the volume enclosed by the canopy. The outer surface of the volume is expanding at the rate $\mathrm{d}r_c/\mathrm{d}t$, and the front and rear surfaces are moving at speeds u_c and $u_c+\mathrm{d}r_c/\mathrm{d}t$, respectively, relative to the inertial axes. The mass flux velocities are u_i, u_x, and u_r at the various surfaces, and are assumed constant over each surface.

The net fluid velocity at the canopy is assumed to be of the form

$$u_m=\bar{\lambda}\left(u_c+\frac{\mathrm{d}r_c}{\mathrm{d}t}\right)+\lambda u_x \tag{16}$$

For nonporous materials, the fluid in contact with the canopy is at rest relative to the canopy. For porous materials, u_x is the velocity of the fluid passing through the material, measured relative to the inertial axes.

Similarly, the radial velocity of the fluid is assumed to vary linearly as

$$u_r=\left(\frac{\mathrm{d}r_c}{\mathrm{d}t}+\lambda u_R\right)\left(\frac{r}{r_c}\right) \tag{17}$$

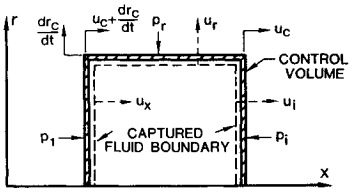

Fig. 4 Control volume for captured fluid.

Again, for a nonporous material, the fluid in contact with the skirt is at rest relative to the skirt. For a porous material, u_R is the velocity of the fluid passing through the skirt, but measured relative to the skirt.

Conservation of mass for the control volume gives

$$\frac{d}{dt}(\rho V)=\pi\rho r_c^2(u_c-u_i)-\pi\rho(r_c^2-r_v^2)\lambda\left(u_c+\frac{dr_c}{dt}-u_x\right)$$

$$-\pi\rho r_c r_s\lambda u_R-\pi\rho r_v^2\left(u_c+\frac{dr_c}{dt}-u_m\right) \tag{18}$$

where V, the volume, is $\pi r_s r_c^2$. Since the vent area is typically 10% or less of the constructed diameter, r_v will be assumed zero in the following. Expanding and nondimensionalizing Eq. (18) results in

$$(2-3R_c+\lambda R_c)\dot{R}_c-\bar{\lambda}R_c v_c+R_c v_i-\lambda R_c v_x+2R_s\lambda v_R=0 \tag{19}$$

This is a kinematic equation, and while it does not define the behavior of any variables, it can be used to compute one in terms of the others. For a nonporous canopy and skirt, Eq. (19) reduces to

$$[2+(\lambda-3)R_c]\dot{R}_c-R_c v_c+R_c v_i=0 \tag{20}$$

Equation (20), together with the equations of change for R_c and v_c, can be used to determine the time variation of v_i, which in turn defines the pressure loading function ΔQ_i, on nonporous canopies.

For porous materials, two other equations are required to determine v_x and v_R, then Eq. (19) can be used to solve for v_i as mentioned above. The necessary relations are conservation of axial and radial momentum for the air mass. Under the assumption of no radial variation in u, the axial momentum is

$$P_x=\pi\rho r_c^2\int_0^{r_s}u\,d\xi \tag{21}$$

Integrating the differential equation for the time rate of change of axial momentum[19] over the canopy volume, and accounting for the fact that the control surface is in motion, results in

$$\frac{dP_x}{dt}=\pi\rho r_c^2 u_i(u_c-u_i)-\pi\rho r_c^2\lambda u_x\left(u_c+\frac{dr_c}{dt}-u_x\right)$$

$$+2\pi\rho r_c\int_0^{r_s}u\left(\frac{dr_c}{dt}-u_r\right)\Big|_{r=r_c}d\xi-2\pi\int_0^{r_c}(p_i-p_1)r\,dr \tag{22}$$

The first term in Eq. (22) represents the axial momentum flux through the inlet of the parachute ($x=x_c$). The second and third terms represent the axial momentum flux through the canopy and skirt, respectively. The final term is the acceleration of the air mass due to pressures acting at the inlet and over the canopy. Using Eq. (17) and definition (21), the third term may be integrated to give

$$2\pi\rho r_c\int_0^{r_s}u\left(\frac{dr_c}{dt}-u_r\right)\Big|_{r=r_c}d\xi=\frac{-2\lambda u_R P_x}{r_c} \tag{23}$$

The remaining integral is easily evaluated under the assumption of no radial variation in axial velocity.

$$-2\pi\int_0^{r_s}(p_i-p_1)r\,dr=-\pi r_c^2[p_i-\lambda p(u_x)-\bar{\lambda}p_0] \tag{24}$$

where p_0 is the stagnation pressure acting on the interior of the canopy, and $p(u_x)$ is the static pressure in the porous openings of the canopy. The final nondimensional form of Eq. (22) is

$$\dot{p}_x=R_c^2 v_i(v_c-v_i)-\lambda R_c^2 v_x(v_c+\dot{R}_c-v_x)$$

$$-(2\lambda v_R p_x)/R_c-R_c^2(Q_i-\lambda Q_x-\bar{\lambda}Q_0) \tag{25}$$

Equation (25) may be integrated in nondimensional time, just as the rigid body equations are, but the flux velocity v_x must be extracted from the momentum term. Using Bernoulli's equation and the assumption of linear axial variation of pressure, it may be shown that

$$p_x=R_s R_c^2\left[v_c-\frac{2}{3}\right.$$

$$\left.\times\left(\frac{(v_c-v_i)^2+(v_c-v_i)(v_c-v_m)+(v_c-v_m)^2}{(v_c-v_m)+(v_c-v_i)}\right)\right] \tag{26}$$

Solving the conservation of mass equation (19) for v_i, inserting in Eq. (26), and solving the resulting quadratic expression for v_c-v_m gives

$$v_c-v_m=[-B+\sqrt{B^2-4AC}]/2A \tag{27a}$$

where

$$A=2(1+\lambda+\lambda^2) \tag{27b}$$

$$B=2D(1+2\lambda)-3(1+\lambda)w \tag{27c}$$

$$C=D(2D-3w) \tag{27d}$$

$$D=\frac{(2-3R_c)\dot{R}_c+2R_s\lambda v_R}{R_c} \tag{27e}$$

and

$$w=v_c-p_x/R_s R_c^2 \tag{27f}$$

Equations (27) and the nondimensional form of Eq. (16) yieid the net fluid velocity v_m at the canopy, the flux velocity v_x, and hence the pressures. Note, however, that an equation for v_R is still required. The same procedure used to derive Eq. (26) may be used for the radial momentum of the air mass, resulting in

$$\dot{p}_r=p_r\frac{[(2-\lambda)R_s-R_c]\dot{R}_c}{R_s R_c}-\tfrac{2}{3}\bar{\lambda}R_c R_s\dot{R}_c \tag{28}$$

The radial flux velocity is then

$$v_R=\frac{3p_r}{2R_s R_c^2}-\dot{R}_c \tag{29}$$

The entire system of equations is formed by determining expressions for the pressure and pressure loading functions. These expressions are found using Bernoulli's equation written with respect to a moving surface. The nondimensional

functions in Eq. (25) are easily shown to be

$$Q_i \equiv \frac{P_i - P_\infty}{\frac{1}{2}\rho_\infty V_\infty^2} = v_c^2 - (v_c - v_i)^2 \tag{30}$$

and similarly,

$$Q_x = (v_c + \dot{R}_c)^2 - (v_c + \dot{R}_c - v_x)^2 \tag{31}$$

$$Q_0 = (v_c + \dot{R}_c)^2 \tag{32}$$

The pressure loading functions necessary for Eqs. (10) and (14) are somewhat more complicated since differential pressures are required, and these differ for porous and nonporous surfaces. The differential loading for the canopy will be developed first. If the canopy is nonporous, the interior pressure is the stagnation pressure for a surface normal to a flow moving with speed $u_c + dr_c/dt$. The opposing pressure is assumed to be freestream static in the present case. The loading is then given by

$$\Delta Q_c = (v_c + \dot{R}_c)^2 \tag{33}$$

Although ΔQ_c actually varies over the surface, experimental observations indicate that this is a good average value for the loading.

For porous canopies such as a ribbon parachute, the differential loading varies across the surface from pore to pore. Again assuming that the wake pressure is freestream, the loading is

$$\Delta Q_c = (\pi/4) Q_0 \tag{34}$$

In Eq. (34), the loading across a ribbon is assumed to vary elliptically and to be zero at the ribbon edge (similar to the tip of a thin wing).

For the nonporous skirt, the differential loadings are

$$\Delta Q_i = Q_i - \dot{R}_c^2 \tag{35}$$

and

$$\Delta Q_s = Q_0 - \dot{R}_c^2 \tag{36}$$

at the inlet and at the skirt-canopy juncture, respectively. Equations (35) and (36) are derived very straightforwardly by writing Bernoulli's equation in a coordinate system on the skirt.

The porous skirt represents the biggest problem. First, the outer pressure is not known or easily approximated as in the nonporous case. Secondly, the flow through the ribbons or pores affects outer pressures. For this analysis, it is assumed that porosity can be accounted for by assuming that the pores are gaps between ribbons, with the ribbons modeled as ideal two-dimensional airfoils. The net normal loading coefficient per unit area is then

$$C_N = 2\pi \sin\alpha \tag{37}$$

where

$$\tan\alpha = v_R/(v_c - v) \tag{38}$$

v_c is the nondimensional axial velocity of the skirt and v is the local fluid axial velocity. Thus

$$\Delta Q_i = q_{\text{rel}_i} 2\pi \sin\alpha_i \tag{39}$$

and

$$\Delta Q_s = q_{\text{rel}_s} 2\pi \sin\alpha_s \tag{40}$$

where the q_{rel}'s are the nondimensional relative dynamic pressures.

Results

The inflation history for an infinite mass, nonporous model parachute is given in Fig. 5, with experimental data from Ref. 20. The inflation curve is initially flat while the captured air mass is being accelerated. The curve then attains a steep, almost linear, shape as filling continues, with a slight overinflation before steady state is reached. Fill times are shown in the accompanying legend, which includes the variation for the separate runs from Ref. 20. The low-amplitude, low-frequency, damped oscillations of the present method makes the steady state difficult to define. The oscillations have essentially died out for τ between 3.5 and 4.0, which agrees well with the fill times from both experiment and Pepper's equation.[1] The predicted steady-state diameter is larger than experiment by about 10%. However, if the cylinder is equated to a hemisphere of the same surface area, the result is much closer to experiment.

Several test cases were used to investigate the effects of parameter variation on the finite mass inflation of nonporous canopies; classical results are shown in Figs. 6 and 7. In Fig. 6, the results of doubling suspension line length are shown. The change has no significant influence on the inflation time; however, a larger steady-state radius is obtained.

The influence of varying canopy initial conditions is shown in Fig. 7. The smooth, well-behaved curve is for canopy and air mass initial velocities equal to forebody initial velocity (no

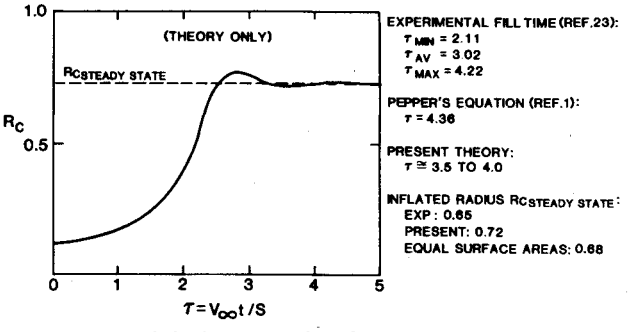

Fig. 5 Inflation comparison for nonporous canopy.

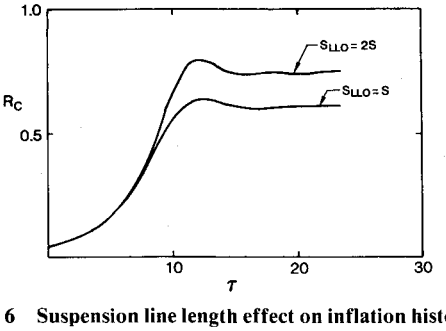

Fig. 6 Suspension line length effect on inflation history.

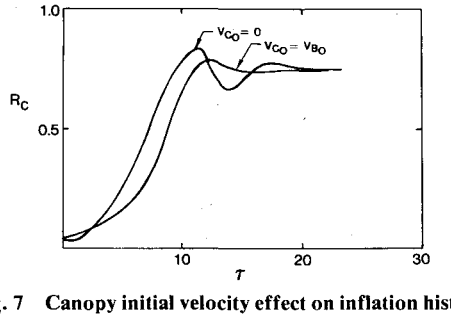

Fig. 7 Canopy initial velocity effect on inflation history.

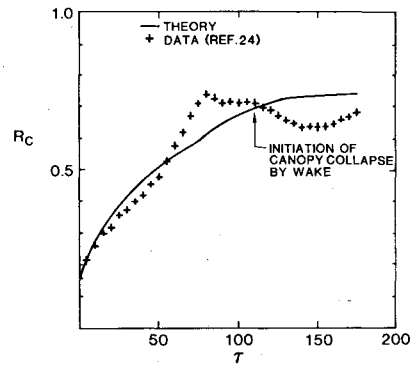

Fig. 8 Low-speed inflation comparison for 46-ft ribbon chute.

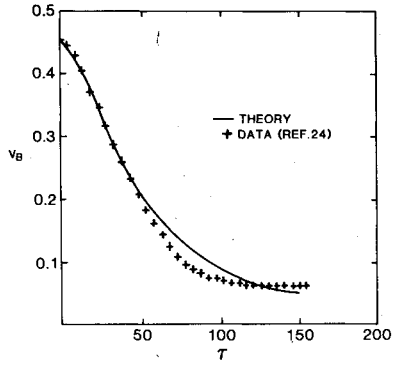

Fig. 9 Forebody deceleration comparison, 46-ft ribbon chute.

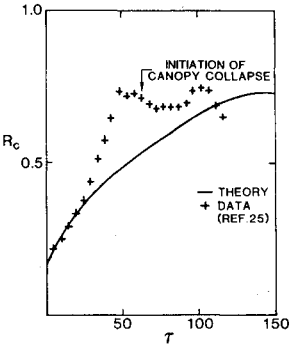

Fig. 10 High-speed inflation comparison for 46-ft ribbon chute.

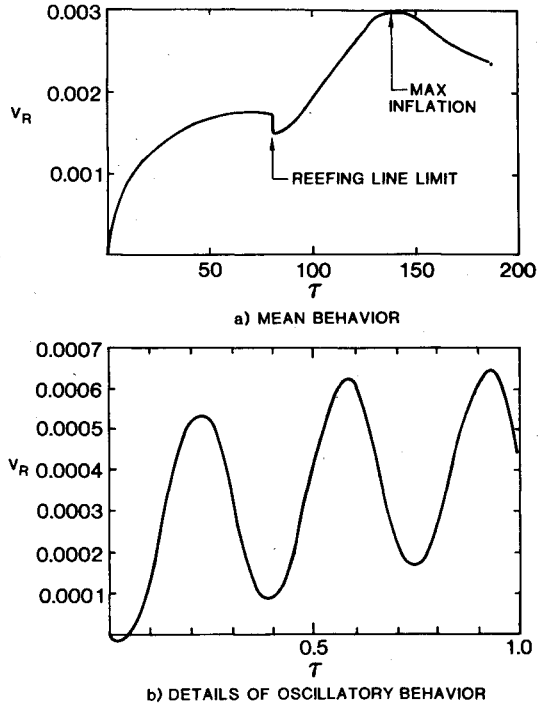

Fig. 11 Predicted radial flux velocity, 46-ft ribbon chute.

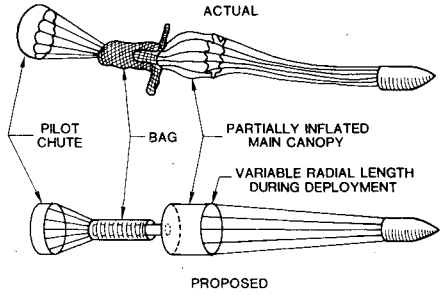

Fig. 12 Deployment simulation using present model.

initial relative motion). The highly perturbed curve was produced by setting the initial velocities of the canopy and air mass to zero. Note the slight deinflation as the canopy and air mass are snatched up to speed. The canopy then inflates much faster than the previous case, with a different shape to the inflation curve, and has a larger maximum inflation. There is a noticeable instability following maximum inflation as part of the accelerating air mass is expelled from the canopy volume. This result implies what has been stated many times in the literature, namely, that initial conditions exert a strong, if not dominant, influence on inflation.

Figures 8-10 present comparisons of some results of the present method with experimental data for a 46-ft-diam ribbon parachute with approximately 25% porosity. The data were taken from Refs. 21 and 22.

The predicted history shown in Fig. 8 has the correct order of magnitude for inflation time, however, the steady-state radius and the detailed shape of the curve are not well predicted. The steady-state radius is slightly larger than experiment, just as in the nonporous case. The inability of the present method to reproduce the exact shape of the curve is due primarily to the geometric model assumed for the canopy, although the unsteady wake is also known to have a significant influence on this particular parachute. The data for forebody deceleration is shown in Fig. 9. Considering the coarseness of the present model and the simplifying assumptions therein, the agreement is probably better than should be expected.

Figure 10 contains results for the same configuration as Figs. 8 and 9 but with a higher initial velocity. The comparison is extremely poor and the expected decrease in inflation time with increased forebody initial velocity was not obtained. The poor comparison may be due to the fact that the incompressibility assumption of the analysis was violated, since the initial velocity was nearly sonic. The porous canopy model was found, through numerical experiment, to be extremely sensitive to the initial conditions imposed on the canopy, suspension lines, and captured air mass. With proper choice of initial conditions for these parameters, results could be obtained with the same accuracy and agreement as shown in Fig. 8. Unfortunately, it is not possible at present to select these conditions a priori.

Figure 11 presents some typical results for the net radial outflow velocity during inflation. A high-frequency fluctuation is predicted, similar to the ribbon flutter phenomena observed during inflation of ribbon parachutes. This oscillation in v_R also affects the differential pressure loading in the model, again implying ribbon flutter, but also indicating that some of the fluctuations in differential pressure measurements may not be noise at all.

Conclusions

A simple analytical model for predicting parachute inflation has been developed, without recourse to experimental inputs. The model includes both rigid body dynamics and fluid kinetics. The inclusion of fluid kinetics provides a method for examining the important effects of the captured fluid mass, for isolating and examining parameters causing specific behavior during inflation, and for developing scaling parameters. The successful coupling of fluid kinetics with parachute and forebody dynamics in the present method implies that an expanded finite-element model is feasible and may be developed without recourse to experimental inputs.

Inflation times and inflation radius histories are reasonably well predicted when the correct initial conditions (terminal conditions for the deployment stage) are provided. The results were found to be extremely initial condition dependent, particularly for ribbon parachutes, and this further emphasizes the need for accurate deployment models which include fluid kinetics. Figure 12 illustrates schematically how the present model might be modified to simulate deployment.

Acknowledgment

This work was supported by the Department of Energy.

References

[1] Pepper, W. B. and Maydew, R. C., "Aerodynamic Decelerators—An Engineering Review," *Journal of Aircraft,* Vol. 8, Jan. 1971, pp. 3-19.

[2] Roberts, B. W. and Reddy, K. R., "A Discussion of Parachute Inflation Theories," AIAA Paper 75-1351, 1975.

[3] Ewing, E. G., Bixby, H. W., and Knacke, T. W., "Recovery Systems Design Guide," AFFDL-TR-78-161, Dec. 1978.

[4] Muller, W., "Parachutes for Aircraft," NACA-TM-450, 1927.

[5] Scheubel, F. N., "Notes on Opening Shock of a Parachute," Progress Report No. IRE-65, Foreign Exploitation Section, April 1946.

[6] O'Hara, F., "Notes on the Opening Behavior and the Opening Forces of Parachutes," *Royal Aeronautical Society Journal,* Vol. 53, Nov. 1949, pp. 1053-1062.

[7] Heinrich, H. G., "A Linearized Theory of Parachute Opening Dynamics," *Aeronautical Journal,* Vol. 76, Dec. 1972, pp. 723-731.

[8] Wolf, D., "A Simplified Dynamic Model of Parachute Inflation," AIAA Paper 73-450, May 1973.

[9] Weinig, F. S., "On the Dynamics of the Opening Shock of a Parachute," TR-6, USAF Office of Aeronautical Research, Wright Air Development Center, Ohio, Feb. 1951.

[10] Toni, R. A., "Theory on the Dynamics of a Parachute System Undergoing Its Inflation Process," AIAA Paper 70-1170, Sept. 1970.

[11] McVey, D. F. and Wolf, D. F., "Analysis of Deployment and Inflation of Large Ribbon Parachutes," *Journal of Aircraft,* Vol. 11, Feb. 1974, pp. 96-103.

[12] Fu, K.-H., "Theoretical Investigation of the Opening Process in a Flexible Parachute-Load System," Deutsche Luft-und Raumfahrt, Forschungsbericht 75-56, Deutsche Forschungs-und Versuchsanstalt für Luft-und Raumfahrt, Braunschweig, Germany, Aug. 1975.

[13] Roberts, B. W., "Aerodynamic Inflation of Shell Type Parachute Structures," *Journal of Aircraft,* Vol. 11, July 1974, p. 390.

[14] Klimas, P. C., "Internal Parachute Flows," *Journal of Aircraft,* Vol. 9, April 1972, pp. 313-314.

[15] Klimas, P. C., "Inflating Parachute Canopy Differential Pressures," *Journal of Aircraft,* Vol. 16, Dec. 1979, p. 861.

[16] Reddy, K. R. and Roberts, B. W., "Inflation of a Multi-Element Parachute Structure," AIAA Paper 75-1353, Nov. 1975.

[17] Payne, P. R. and Band, E. G. U., "Final Report—Research on Parachute Opening," Payne, Inc., Working Paper 145-13, Annapolis, Md., Nov. 1976.

[18] Wilcox, B., "The Calculation of Filling Time and Transient Loads for a Parachute Canopy During Deployment and Opening," Sandia Corporation Research Rept. SC-4151(TR), Feb. 1958.

[19] Bird, R. B., Stewart, W. E., and Lightfoot, E. N., *Transport Phenomena,* John Wiley and Sons, 1960, pp. 83-91.

[20] Klimas, P. C. and Rogers, D. F., "Helium Bubble Survey of a Parachute-Opening Flowfield Using Computer Graphics Techniques," *Journal of Aircraft,* Vol. 14, Oct. 1977, pp. 952-958.

[21] Simpson, S. L., "Data Reduction Report—Sandia Test R722016," Tonopah Test Range, Sandia National Laboratories, July 1980.

[22] Pedro, E. L., "Data Reduction Report—Sandia Test R722810, Area III, Sandia National Laboratories, June 1980.